Electrocatalytic reduction of CO2 and nitrate on immobilized metal porphyrins

Shen, Jing

Appendix A: Supplementary Material for Chapter 2

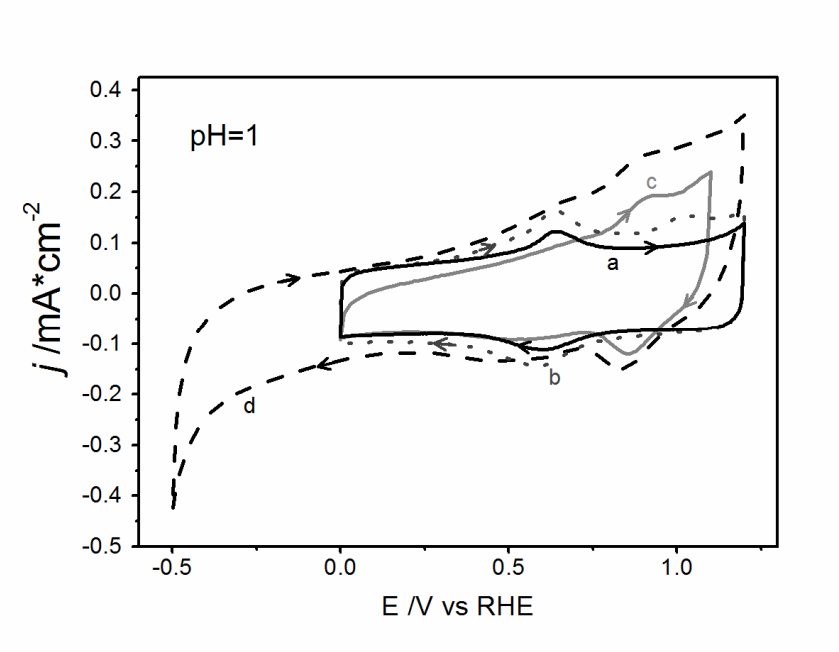

Figure 1. Characterization of immobilized cobalt protoporphyrin electrode. The cyclic voltammogram of: (a) pyrolytic graphite electrode; (b) pyrolytic graphite electrode with 100 μL 0.5 mM cobalt protoporphyrin solution in electrolyte; (c) cobalt protoporphyrin immobilized pyrolytic graphite electrode and (d) cobalt protoporphyrin immobilized pyrolytic graphite electrode scanned to more negative potential. All voltammograms obtained in 0.1 M $HClO_4$ solution; scan rate is 500 mVs^{-1}. From the peak corresponding to the Co^{III}/Co^{II} redox couple at 0.8-0.9 V (with due account of the capacitive background current), the coverage of cobalt protoporphyrin can be estimated as $4x10^{-10}$ mol cm^{-2}. The cleanliness of the solution was verified by blank voltammetry of a platinum electrode, which showed no impurities.

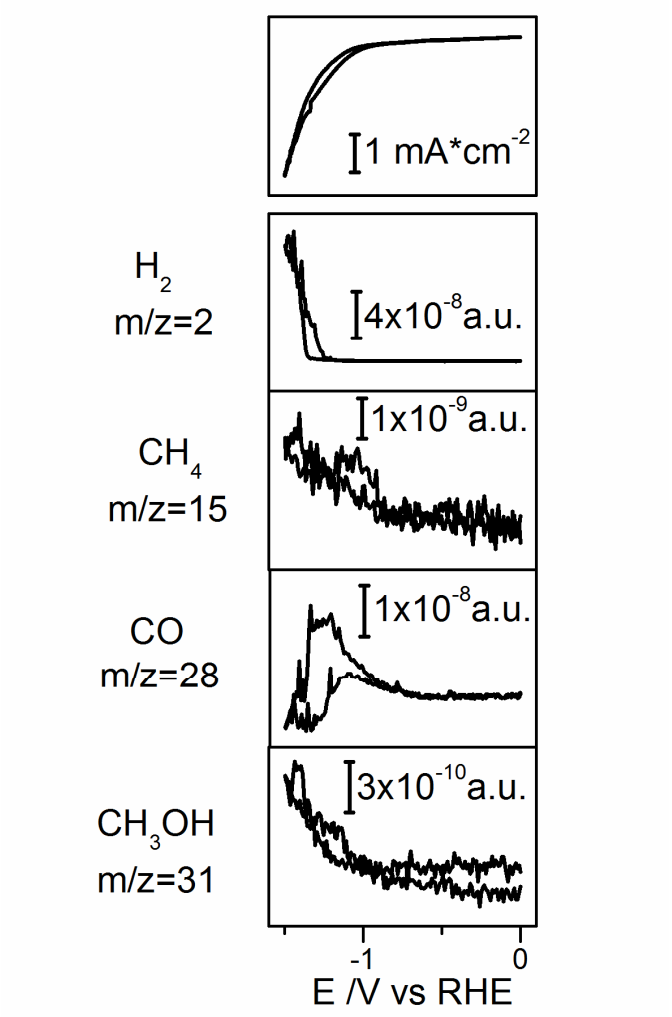

Figure 2. Cyclic voltammetry combined with OLEMS measurement of electrochemical reduction of CO_2 on a cobalt-tetramethoxyphenylporphyrin modified pyrolytic graphite electrode in 1 mM $HClO_4$ + 99 mM $NaClO_4$ (pH=3) solution, showing the cyclic voltammetry (upper panel) and the hydrogen, methane and methanol formation (lower panels). This experiment demonstrates that a small amount of alcohol (m/z=31) is produced from the CO_2 reduction catalyzed by the cobalt porphyrin. From the absence of higher alcohols C2 signals, we conclude that m/z=31 must correspond to methanol.

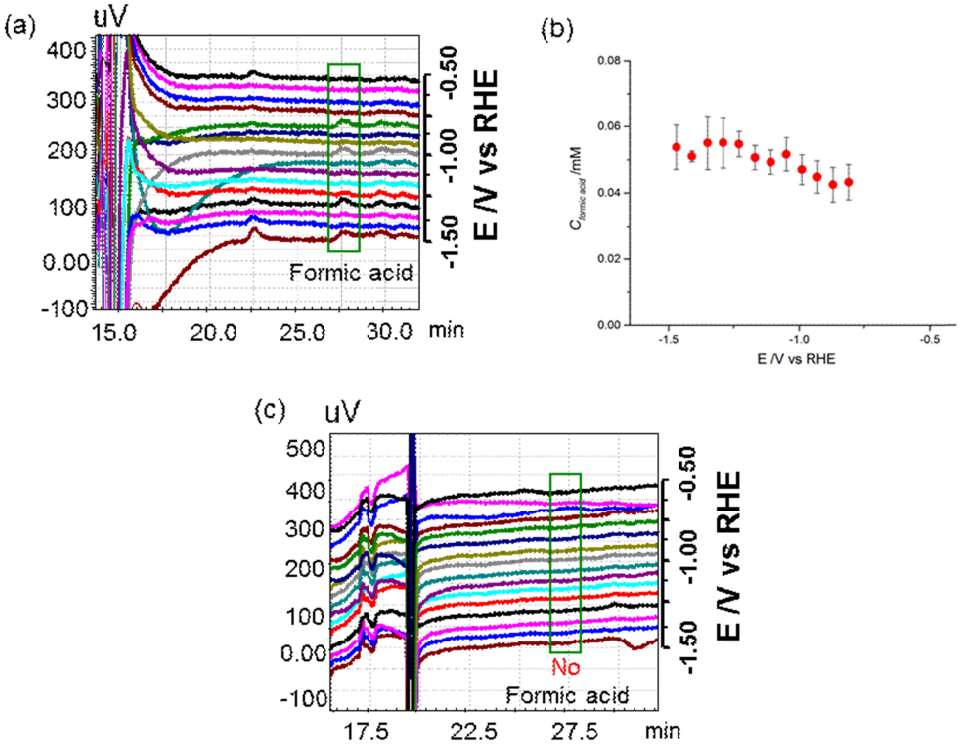

Figure 3. Liquid products detected using HPLC. (a) Chromatograms obtained during the electrochemical reduction of CO_2 on the CoPP-PG electrode in 0.1 M $HClO_4$ solution vs potential, which were collected every 60 mV. (b) The corresponding concentration of formic acid vs potential at pH=1; error bars determined from 3 separate experiments. (c) Chromatograms for electrochemical reduction of CO_2 on the CoPP-PG electrode in 1 mM $HClO_4$+ 99 mM $NaClO_4$ solution vs potential, which were collected every 60 mV, showing the absence of formation of formic acid at pH=3. The fluctuations of the detected HCOOH in Fig.(b) are due to the very small amount of formic acid formed from CO_2 electrochemical reduction in combination with the hydrogen formation and sample collection.

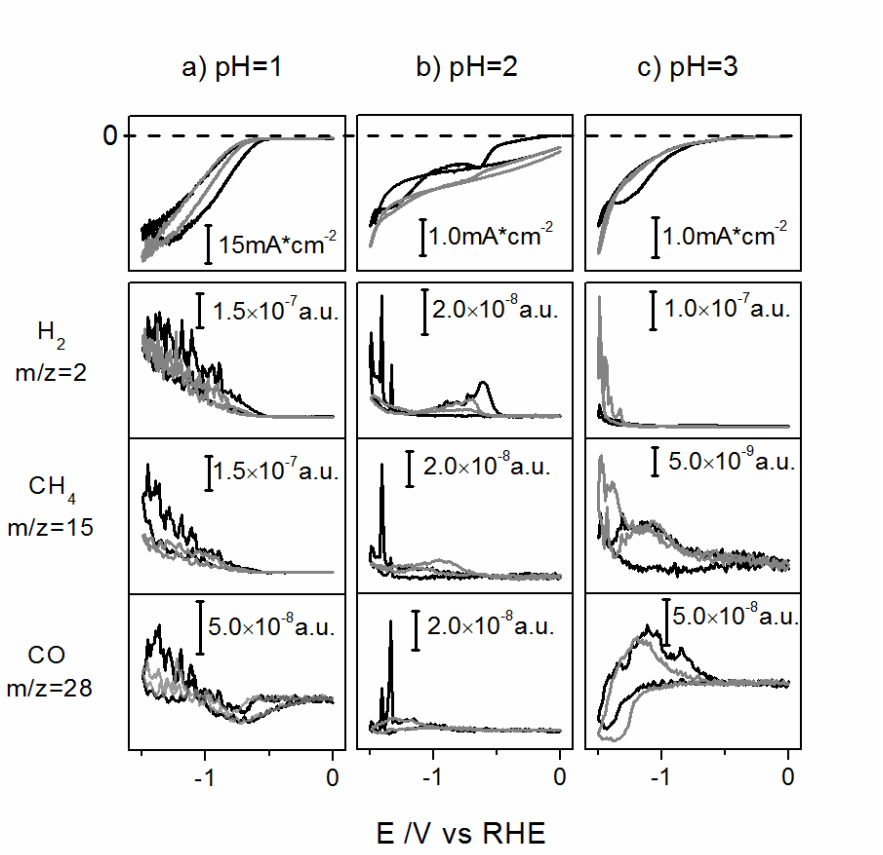

Figure 4. Voltammetry and the unnormalized signals of the volatile product identification by OLEMS during the electrochemical reduction of CO_2 on cobalt protoporphyrin immobilized pyrolytic graphite electrode. (a) 0.1 M $HClO_4$. (b) 10 mM $HClO_4$ + 90 mM $NaClO_4$ and (c) 1 mM $HClO_4$ + 99mM $NaClO_4$; showing first cycle (black curve) and second cycle (gray curve). Top panels: cyclic voltammetry. Lower panels: associated OLEMS mass signals for m/z=2 (H_2), 15 (CH_4) and 28 (CO). Scan rate in all cases 1 mV s^{-1}.

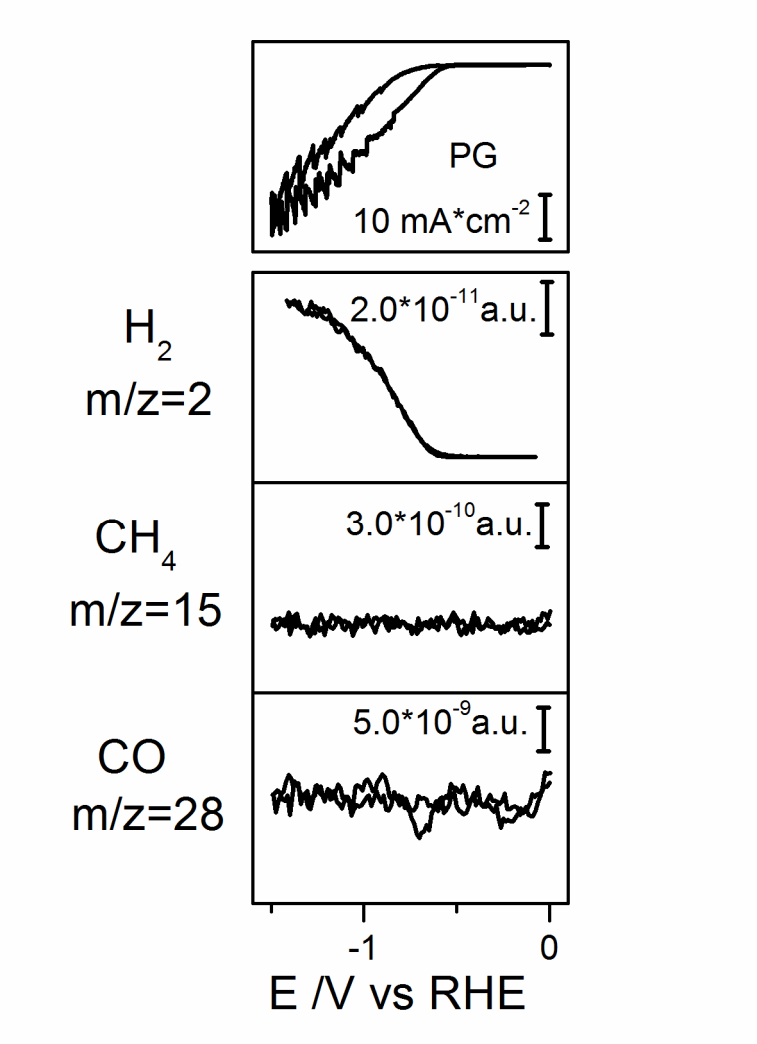

Figure 5. Combined CV-OLEMS measurement of electrochemical reduction of CO_2 on an unmodified pyrolytic graphite electrode in 0.1 M $HClO_4$ solution, showing the cyclic voltammetry (upper panel) and the hydrogen, methane, and carbon monoxide formation (lower panels). This experiment demonstrates that the catalytic activity towards CO_2 reduction is not from pyrolytic graphite.

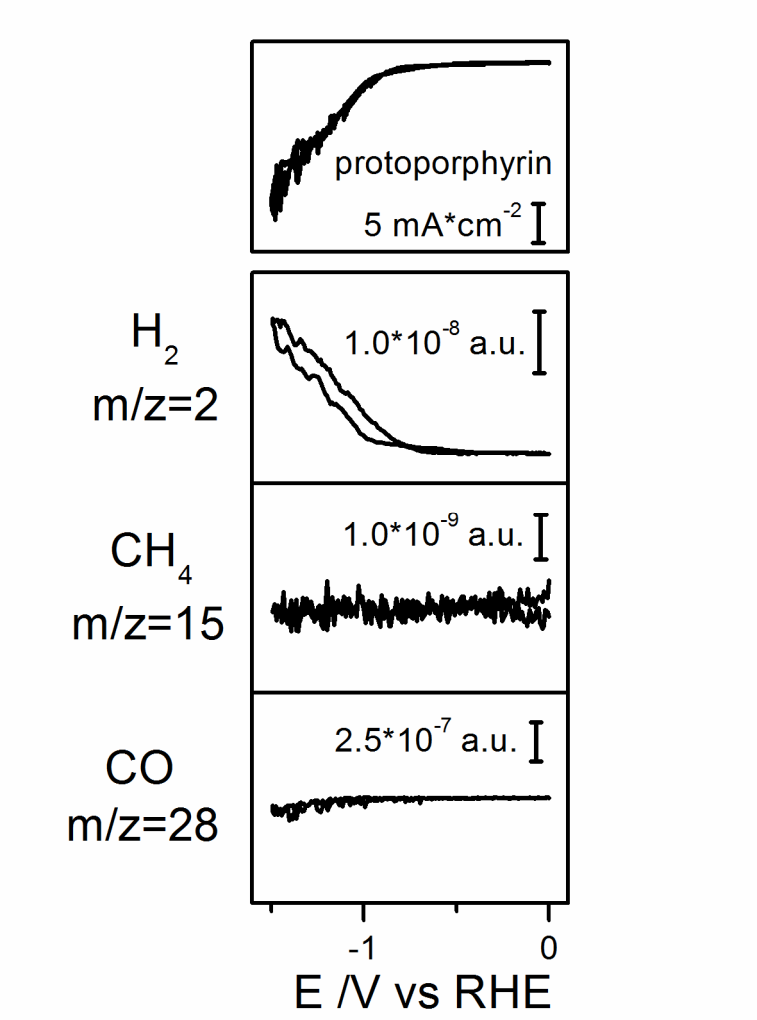

Figure 6. Combined CV-OLEMS measurement of electrochemical reduction of CO_2 on cobalt-free protoporphyrin modified pyrolytic graphite electrode in 0.1 M $HClO_4$ solution, showing the cyclic voltammetry (upper panel) and the hydrogen, methane and carbon monoxide formation (lower panels). This experiment demonstrates that the catalytic activity for CO_2 reduction comes from the interaction of the cobalt metal center and protoporphyrin ring.

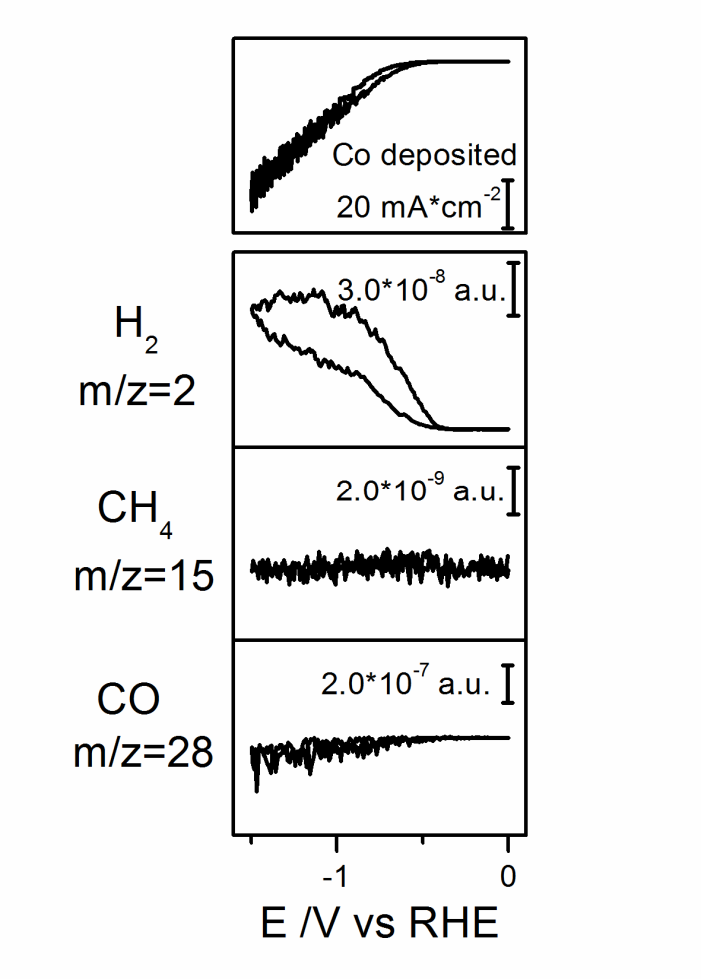

Figure 7. Combined CV-OLEMS measurement of electrochemical reduction of CO_2 on a cobalt electrodeposited pyrolytic graphite electrode in 0.1 M $HClO_4$ solution, showing the cyclic voltammetry (upper panel) and the hydrogen, methane and carbon monoxide formation (lower panels). This experiment demonstrates that the catalytic activity for CO_2 reduction is not from the cobalt released from cobalt protoporphyrin. The deposition of cobalt was conducted using the same procedure as described elsewhere[1]. The solution used for cobalt electrodeposition was 3.5 mM $CoCl_2$ in 1 M NH_4Cl solution (pH=4.5). Electrochemical experiments were conducted in a one-compartment three-electrode electrochemical cell with a pyrolytic graphite electrode (diameter:5mm) as working electrode, a graphite rod as a counting electrode and a KCl saturated Ag/AgCl electrode as a reference electrode, to which all potentials here were referred. Cyclic voltammetry was conducted from 0.4 V to -1.3 V to verify the electrochemistry of the working electrode in the electrodeposition bath, after which a current-time transient experiment was conducted by starting the potential at 400 mV for 60s, and jumping to first potential step at -1.3 V for 2s with an interval of 0.2s.

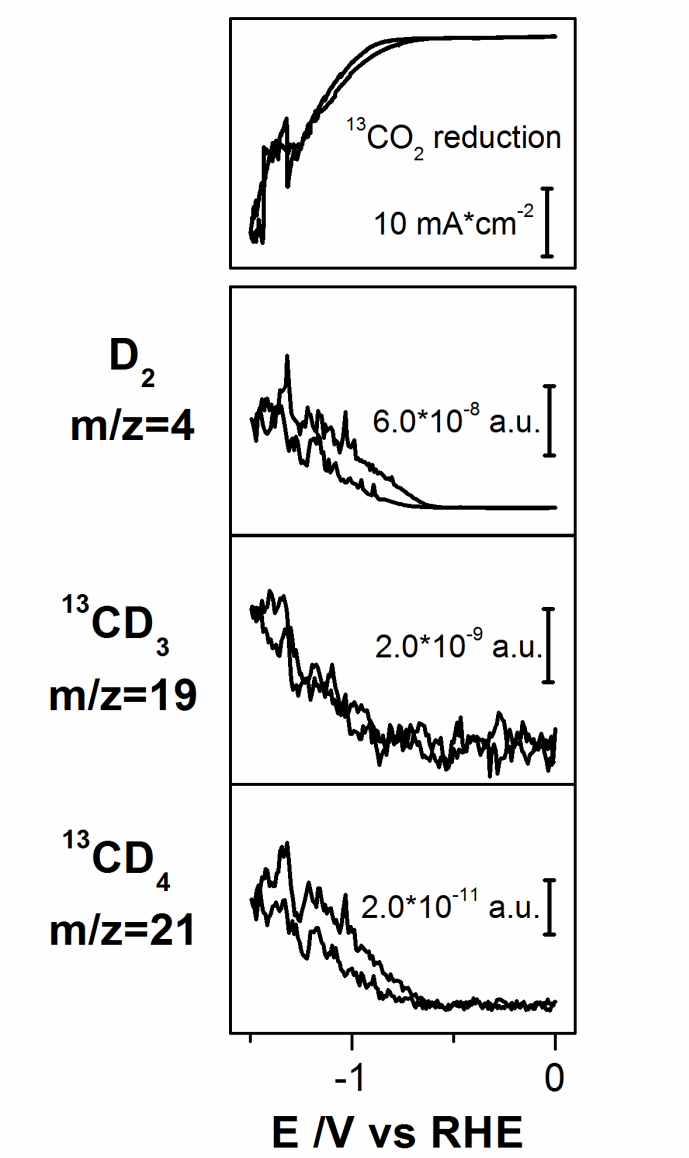

Figure 8. Combined CV-OLEMS measurement of electrochemical reduction of $^{13}CO_2$ on cobalt protoporphyrin modified pyrolytic graphite electrode in 0.1 M $DClO_4$ + D_2O solution, showing the cyclic voltammetry (upper panel) and the hydrogen and methane formation (lower panels). This experiment proves that the catalytic activity of cobalt protoporphyrin and the formation of methane are from dissolved CO_2. m/z=19 corresponds to $^{13}CD_3$; m/z=21 corresponds to $^{13}CD_4$.

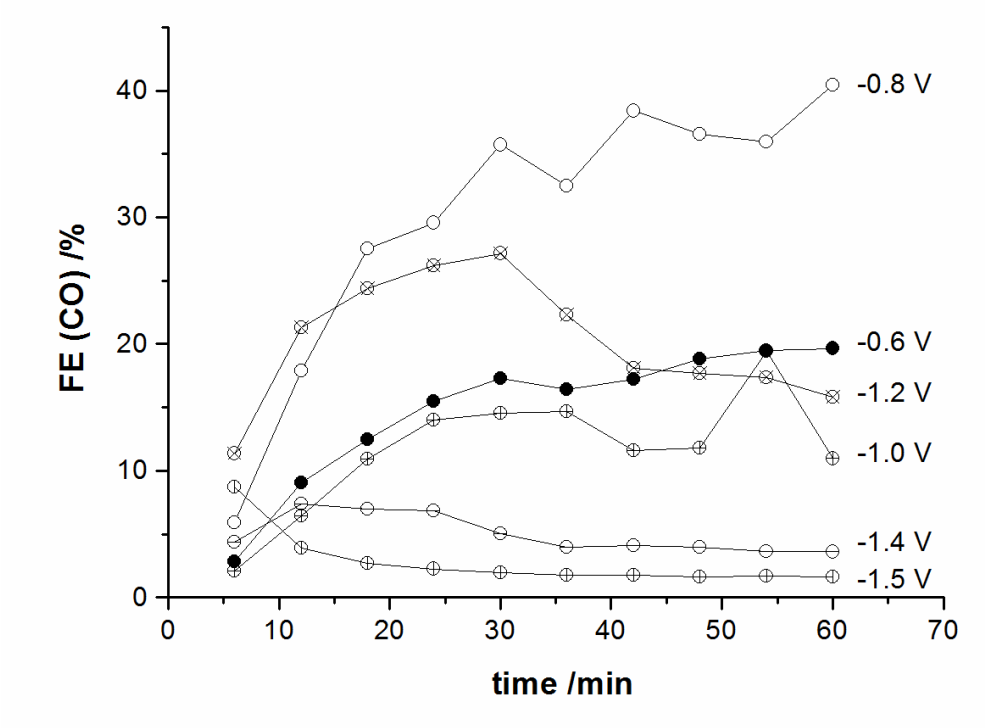

Figure 9. Faradaic efficiency (FE) of CO from controlled potential electrolysis of CO_2 electrochemical reduction on cobalt protoporphyrin modified pyrolytic graphite electrode at different potentials vs RHE as a function of time. Solution: 1 mM $HClO_4$ + 99 mM $NaClO_4$ (pH=3); CO_2 pressure: 1 atm.

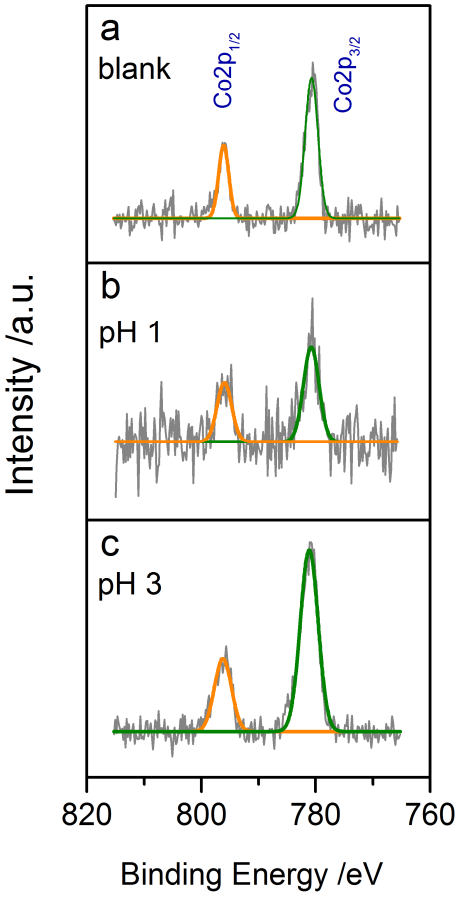

Figure 10. XPS spectra of (a) freshly prepared cobalt protoporphyrin immobilized PG electrode; (b) cobalt protoporphyrin immobilized PG electrode after electrolysis at -1.5 V in 0.1 M $HClO_4$ solution (pH = 1) for 1 hour and (c) cobalt protoporphyrin immobilized PG electrode after electrolysis at -0.8 V in 99 mM $NaClO_4$ + 1 mM $HClO_4$ solution (pH = 3) for 1 hour. Figure (b) and (c) show that the CoPP remains intact on the electrode after electrolysis at very negative potentials. X-ray photoelectron spectroscopy (XPS) spectra were collected on a Quantera SXM (Scanning XPS microprobe) spectrometer equipped with Al Kα (1486.6 eV) X-ray source. The source was operated with a 25 W emission power, beam size of 200 μm and pass energy of 224 eV. The resolution of the spectrometer was 0.2eV and 0.8 eV for high resolution element scan and survey spectra, respectively.

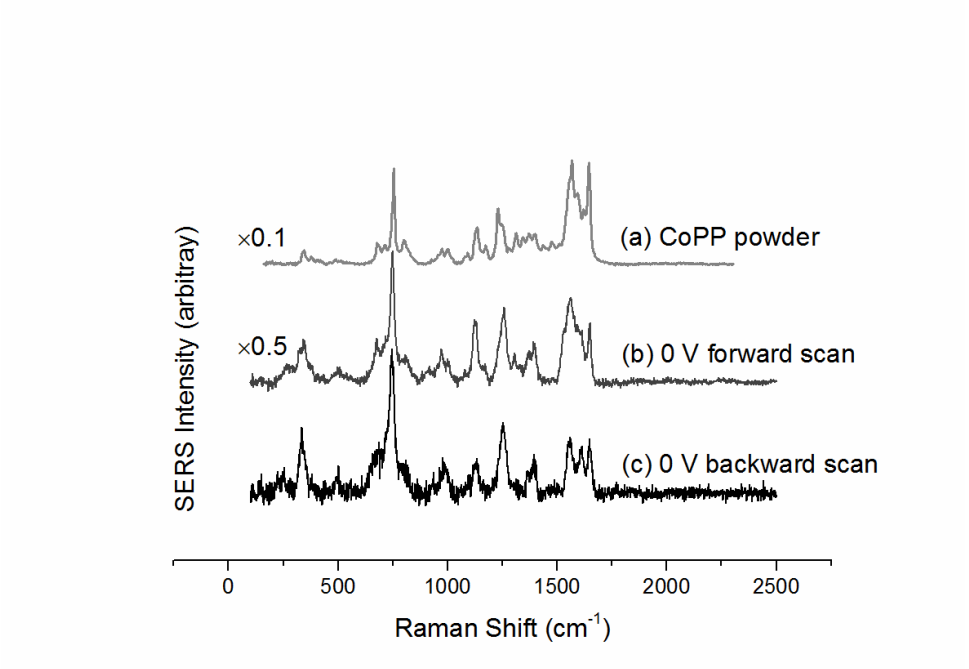

Figure 11. SERS spectra of (a) cobalt protoporphyrin powder; (b) cobalt protoporphyrin immobilized Au electrode at 0 V before scanning and (c) cobalt protoporphyrin immobilized Au electrode at 0 V after voltammetry scanned to negative potentials. Au nano particles were synthesized as in reference[2], which were drop-cast onto a clean Au electrode. The electrode was then dipped into 0.5 mM cobalt protoporphyrin solution to saturate the surface with porphyrin. Cobalt protoporphyrin immobilized electrode was held at different potentials started from 0 V to – 1.5 V vs RHE with 100 mV interval and then back while SERS spectra was collected at each potential.

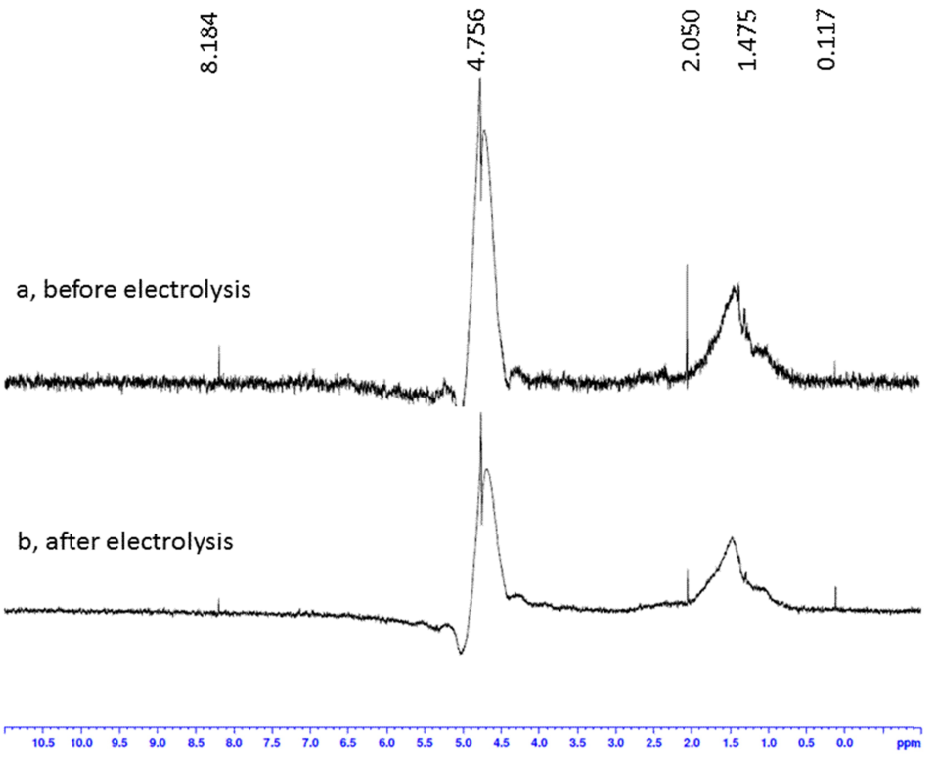

Figure 12. NMR spectra of electrolyte (a) before and (b) after long-term electrolysis in CO_2 saturated 0.1 M $HClO_4$ solution on CoPP immobilized PG electrode. The electrolysis was conducted for 5 hours in a H-cell with 15 mL volume in each compartment. 100 uL solution in working electrode compartment was collected after electrolysis for NMR measurement.

Reference:

1. Kwon Y, Koper M.T.M. Combining Voltammetry with HPLC: Application to Electro-Oxidation of Glycerol. *Anal. Chem.* **2010**, 82(13): 5420-5424.
2. Palomar-Pardavé M, Scharifker BR, Arce EM, Romero-Romo M. Nucleation and diffusion-controlled growth of electroactive centers: Reduction of protons during cobalt electrodeposition. *Electrochim. Acta*. **2005**, 50(24): 4736-4745.

Appendix B: Supplementary Material for Chapter 3

Table 1: Binding energies for low and high spin states and relative energies of the high spin states (vs low spin states) for calculated negatively charged intermediates.

	Low Spin /eV	High Spin /eV	Relative Values /eV*
CoP	-260.03 (1)***	-259.17 (3)	0.86
CoP-CO_2	-282.74 (1)	-281.71 (3)	1.03
CoP-COOH	-285.38 (2)	-284.76 (4)	0.62
CoP-OCHO	-286.18 (2)	-286.58 (4)	-0.4
CoP-CO	-274.74 (1)	-274.70 (3)	0.04
CoP-CHO	-278.13 (2)	-277.11 (4)	1.02
CoP-COH	-276.06 (2)	-275.48 (4)	0.58
CoP-CH_2O	-282.27 (1)	-281.34 (3)	0.93
CoP-CH	-268.49 (2)	-268.26 (4)	0.23
CoP-CH_2	** (1)	-268.54 (3)	**
CoP-CH_3	-278.73 (2)	-278.02 (4)	0.71
CoP-CH_2OH	-285.20 (2)	-284.35 (4)	0.85
CoP-OCH_2O	-287.98 (1)	-287.52 (3)	0.46
CoP-OCH_2	-281.88 (1)	-281.22 (3)	0.66
CoP-OCH_3	-285.81 (2)	-283.42 (4)	2.39
CoP-O	-264.97 (1)	-264.95 (3)	0.02
CoP-OH	-270.20 (2)	-269.88 (4)	0.32
CoP-OCH_2OH	-292.55 (2)	-292.24 (4)	0.31

* Relative values = $E_{\text{high spin}} - E_{\text{low spin}}$

** The close-shell singlet does not converged probably because the lowest singlet configuration is open-shell.

*** The numbers in the brackets are the spin multiplicity.

Table 2: The equilibrium potentials for the formation of the [CoP-COOH] and [CoP-OCHO] intermediates with and without solvation correction.

	E^0 /V_{RHE} Without solvation	E^0 /V_{RHE} With solvation
$[CoP]^0 + CO_2 + H^+ + e^- \longrightarrow [CoP\text{-}COOH]^0$	-0.72	-0.43
$[CoP]^0 + CO_2 + H^+ + e^- \longrightarrow [CoP\text{-}OCHO]^0$	-1.31	-0.92
$[CoP\text{-}CO_2]^- + H^+ + e^- \longrightarrow [CoP\text{-}COOH]^-$	*	-1.01
$[CoP\text{-}CO_2]^- + H^+ + e^- \longrightarrow [CoP\text{-}OCHO]^-$	*	-0.21

* CO_2 cannot bind to CoP without solvation correction, which makes the $[CoP\text{-}CO_2]^-$ is not stable.

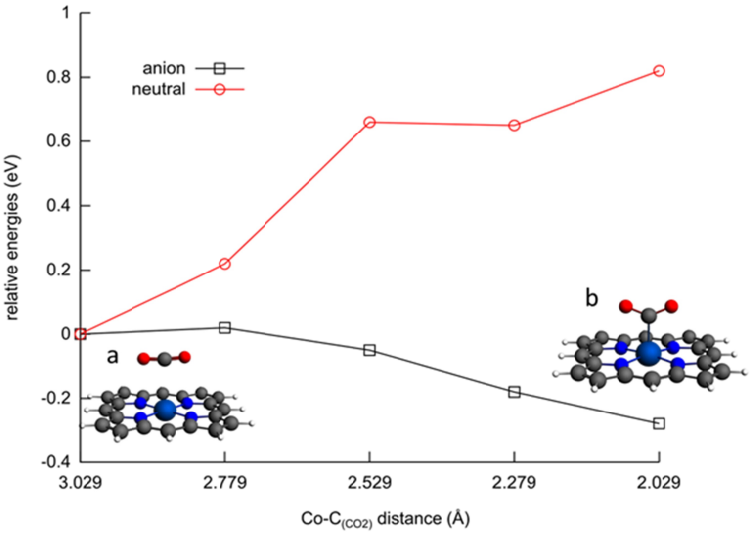

Figure 1. The relative energy of neutral and anionic complexes [Co(P)-(CO_2)] with large Co-$C_{(CO2)}$ distances varies as the CO_2 approaches the metallic center of complex. Inserted Figure (a) is the dissociated CO_2 adduct; inserted Figure (b) is the optimized CO_2 adduct.

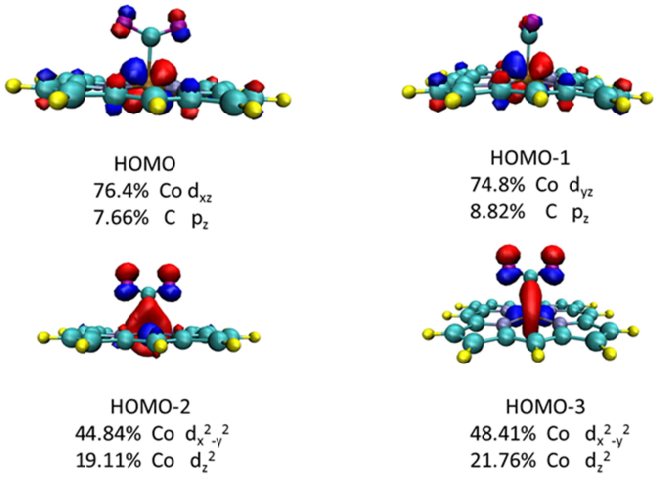

Figure 2. The structures and main contributions of the highest occupied molecular orbitals (HOMO to HOMO-3).